J Mater Sci

Chemical routes to materials

Polyhedral oligomeric silsesquioxane-coated nanodiamonds for multifunctional applications

Shaowei Qin[1,2], Dan Wang[1,*], Jie-Xin Wang[1], Yuan Pu[2,*], and Jian-Feng Chen[1,2]

[1] *Beijing Advanced Innovation Center for Soft Matter Science and Engineering, State Key Laboratory of Organic–Inorganic Composites, Beijing University of Chemical Technology, Beijing 100029, China*

[2] *Research Centre of the Ministry of Education for High Gravity Engineering and Technology, Beijing University of Chemical Technology, Beijing 100029, China*

Received: 30 May 2018
Accepted: 31 July 2018

ABSTRACT

Polyhedral oligomeric silsesquioxane (POSS)-coated nanodiamonds (NDs@POSS) were prepared via the amide formation between amine-functionalized POSS and oxygen-containing groups of NDs. The POSS structures grafted on the surface of NDs enable the NDs@POSS nanocomposites to be well-dispersed in organic solvents and polymers for multifunctional applications. The surface coating of NDs with POSS also bring other incidental advantages such as enhanced thermal stability and superhydrophobic of the NDs. NDs@POSS nanocomposites-embedded hybrid films based on polycarbonate and polyvinyl butyral were fabricated by solution blending methods, showing tunable refractive indexes in the range of 1.49–1.61. Furthermore, the powders of NDs@POSS were superhydrophobic with contact angle of water/air of 154°. Liquid marbles formed by coating the water droplet with NDs@POSS were prepared, and the process intensification effects of the NDs@POSS-based miniature reactors for degradation of methylene and fabrication of Ag nanoparticles were also demonstrated, respectively.

Introduction

Composite materials based on carbon nanomaterials have developed into a very important direction and found many applications in energy and bio-related fields [1–5]. Among them, nanodiamonds (NDs)-embedded hybrid materials are highly attractive and have found their way into many areas [6–8]. For instance, due to the high refractive index (2.42) of the diamond, the NDs exhibit great potential as fillers for the preparation of transparent hybrid films with tunable refractive indexes [9, 10]. However, the commercial available NDs are composed of particle aggregates (size of hundreds of nm), rather than isolated monodisperse nanoparticles [11, 12]. Typically, there are two ways to solve the problem of aggregation of NDs. One is the depolymerization of physical methods such as ball milling [13] and sonic disintegration [14]. It is inevitable to introduce other

Address correspondence to E-mail: wangdan@mail.buct.edu.cn; puyuan@mail.buct.edu.cn

https://doi.org/10.1007/s10853-018-2765-7

Published online: 03 August 2018

impurities by using physical methods for depolymerization of nanodiamonds, which limits their applications [11, 15]. The other route is the modification of the surface chemistry of NDs by using octadecylamine [25], octylamine [16], amino-polyethylene glycol [17] and just to name a few [18, 19], to obtain well-dispersed NDs in solvents. This method has the advantages such as reproducibility and controllability for developing various new NDs with tailor-made structures and well-defined properties [17, 18].

Polyhedral oligomeric silsesquioxane (POSS) is a hybrid inorganic/organic chemical composite, with internal inorganic silicon and oxygen core and eight external organic arms [20, 21]. The diameter of these eight siloxyhexane is 1.2–1.4 nm, and there are functional groups in each octant in Cartesian space, opposite or orthogonal to each other [22]. POSS is highly soluble in many organic/inorganic solvents [20]. The cage-structured POSS is normally considered to be a kind of monodisperse silica with cube inorganic core [23, 24]. Due to its unique nano size structure, high chemical stability and thermal stability and simple chemical modification, POSS has been proved to be an important scaffold for hybrid polymers [25, 26] and used to modify a various types of nanoparticles, such as carbon dots [21], upconversion nanoparticles [27], and iron oxide nanoparticles [28]. The POSS structures grafted on the surface of nanoparticles enable them to be well-dispersed in organic solvents and polymers for multifunctional applications.

Herein, we report the synthesis of POSS-coated nanodiamonds (NDs@POSS) via the amidation reaction between the amine-functionalized POSS and the carboxyl group of ND. Due to the presence of organic groups on POSS structures, the NDs@POSS nanoparticles were able to disperse well in various organic solvents and polymeric matrix. Transparent hybrid films with tunable refractive index were fabricated by solution blending NDs@POSS with polyvinyl butyral (PVB) and polycarbonate (PC), respectively. The hybrid films exhibited enhanced thermal stability than those of pure film. In addition, the powder of NDs@POSS exhibited superhydrophobicity with water/air contact angle of 154°. Liquid marbles coated with NDs@POSS were developed as miniature reactors. The process intensification effects of the NDs@POSS-based miniature reactors for degradation of methylene and fabrication of Ag nanoparticles were demonstrated, respectively.

Experimental

Materials

Powder of NDs with average diameters of < 10 nm, N-methyl pyrrolidone (NMP), ethanol (EAL), methanol (Mt), acetone (Ac), tetrahydrofuran (THF), trichloromethane (TCM), toluene (Tol) and cyclohexane (CX), N,N′-dicyclohexylcarbodiimide (DCC), methylene blue, $NaBH_4$, $AgNO_3$, ammonia and glucose were purchased from Sigma-Aldrich. PC and PVB were obtained from Aldrich to Beijing HWRK Chem Co. Ltd (Beijing China), respectively. Aminopropylisobutyl POSS (POSS-NH_2) was purchased from Hybrid Plastics, Inc. (Hattiesburg, MS, USA). All the chemicals were used as received without further purification and deionized water was used for all experiments.

Surface modification of NDs

The surface functionalization of NDs with carboxy groups were performed by a well-developed thermal oxidation method [29]. Typically, the powder of NDs was dried in a vacuum oven at 80 °C for 2 h to remove the organic impurities and then treated in a furnace at 425 °C under air conditions for 1.5 h, to introduce carboxylic groups on the surface of NDs. The POSS structure was covalently grafted to NDs via the amide formation between the oxygen-containing groups of NDs and amine-functionalized POSS by using DCC as the catalysts (Scheme 1) [21]. Briefly, 1 g powder of POSS-NH_2 were first dissolved to 100 mL THF in a 250 mL round-bottom flask, followed by the addition of 100 mg NDs and 100 mg DCC under ultrasonication treatment. The mixture was then refluxed at 90 °C for 72 h. The NDs@POSS nanocomposites were collected by centrifugation at 10000 rpm for 5 min and then washed by TCM for at least three times to remove the POSS and DCC residues. The precipitates were then dried at 60 °C in a vacuum oven for 2 h to obtain final product of NDs@POSS powder.

Preparation of NDs@POSS-based hybrid films

To prepare the polymer/NDs@POSS nanocomposites as flexible foil, PVB and PC were used as the polymer matrix, respectively. Briefly, 50 mg of PVB was firstly

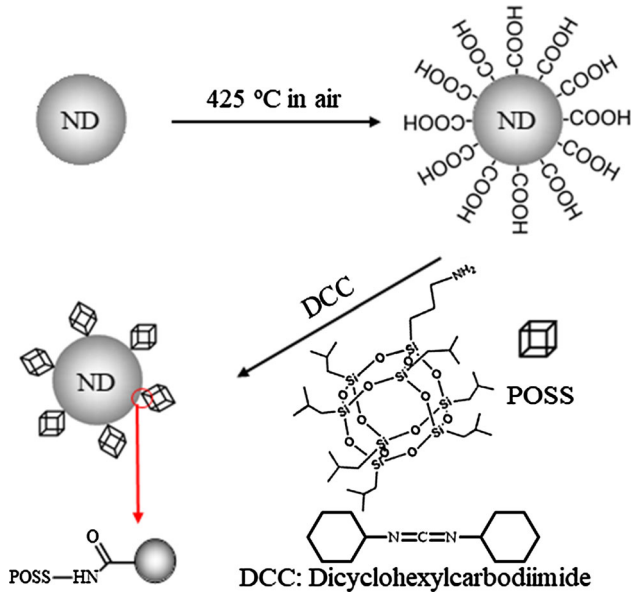

Scheme 1 Schematic showing the route for the carboxyl of NDs and preparation of POSS-coated NDs.

dissolved in 2 mL methanol followed by the addition of a certain amount of NDs@POSS powder. The weight ratios of NDs@POSS to PVB were set as 1, 5, 10, 15 and 20%, respectively. The NDs@POSS-embedded hybrid films with thickness of 0.5 mm were prepared by spin-casting the mixed solution on a glass wafer. The NDs@POSS/PC hybrid films were prepared by similar procedures by using chloroform as the solvent to dissolve PC.

Formation and manipulation of liquid marbles

The obtained NDs@POSS powder was placed in a petri dish and a droplet of aqueous solution deposited onto the powder through pipette tip. By waving the petri dish, a liquid marble could be formed by coating the water droplet with superhydrophobic NDs@POSS powder.

Degradation of methylene blue in liquid marbles

The degradation of methylene blue was carried out in the liquid marble. Briefly, 20 μL aqueous solution of methylene blue (5 mM) was placed on the powder of NDs@POSS. Then 20 μL aqueous solution of $NaBH_4$ was injected into the droplet. The droplet was then coated with NDs@POSS to form a liquid marble. At selected time intervals, the methylene blue solution was extracted out and diluted 100 times in water for UV–Vis spectroscopy measurement. The absorbance intensities of methylene blue at 665 nm were monitored to investigate the reaction kinetics for the degradation of methylene blue in liquid marbles.

Preparation of Ag nanoparticles in liquid marbles

Typically, 1.5 g $AgNO_3$ was dissolved in 8.5 mL water, and then 5 wt% ammonia solution was added under vigorous magnetic stirring until a clear colorless solution was obtained (solution A). 20 μL of solution A were placed on the powder of NDs@POSS, followed by the addition of 20 μL aqueous solution of glucose (10 wt%). The mixture solution was then coated with NDs@POSS to form a liquid marble. After 25 min, the solution inside the liquid marble was extracted out and diluted 100 times in water for transmission electron microscope (TEM) characterization.

Characterization

Powder X-ray diffraction (XRD) patterns were recorded using a Bruker D8 Discover XRD diffractometer equipped with Cu Kα radiation. The thermogravimetric analysis (TGA) results were determined by a NETZSC STA-449C thermogravimetric analyzer with heating rates of 10 °C/min in air. TEM images were obtained by a JEOL JSM-2010F TEM operating with an accelerating voltage of 200 kV. A Malvern Zetasizer Nano ZS90 instrument was used to obtain the dynamic light scattering (DLS) data of the nanoparticles dispersed in toluene. A Nicolet 6700 Fourier transform infrared (FTIR) spectrometer was used to measure the FTIR spectra of the samples. The UV–Vis transmittance spectra were characterized by a Shimadzu UV-2600 UV–Vis spectrometry. The refractive indexes of the films were measured by using an Abbemat 300 automatic refractometer equipped with 589 nm laser.

Results and discussion

Figure 1a, b shows the typical TEM images of ND-COOH and NDs@POSS, respectively. The histograms of the particle size distributions are presented in Fig. 1c, d. For single particle of either ND-COOH or

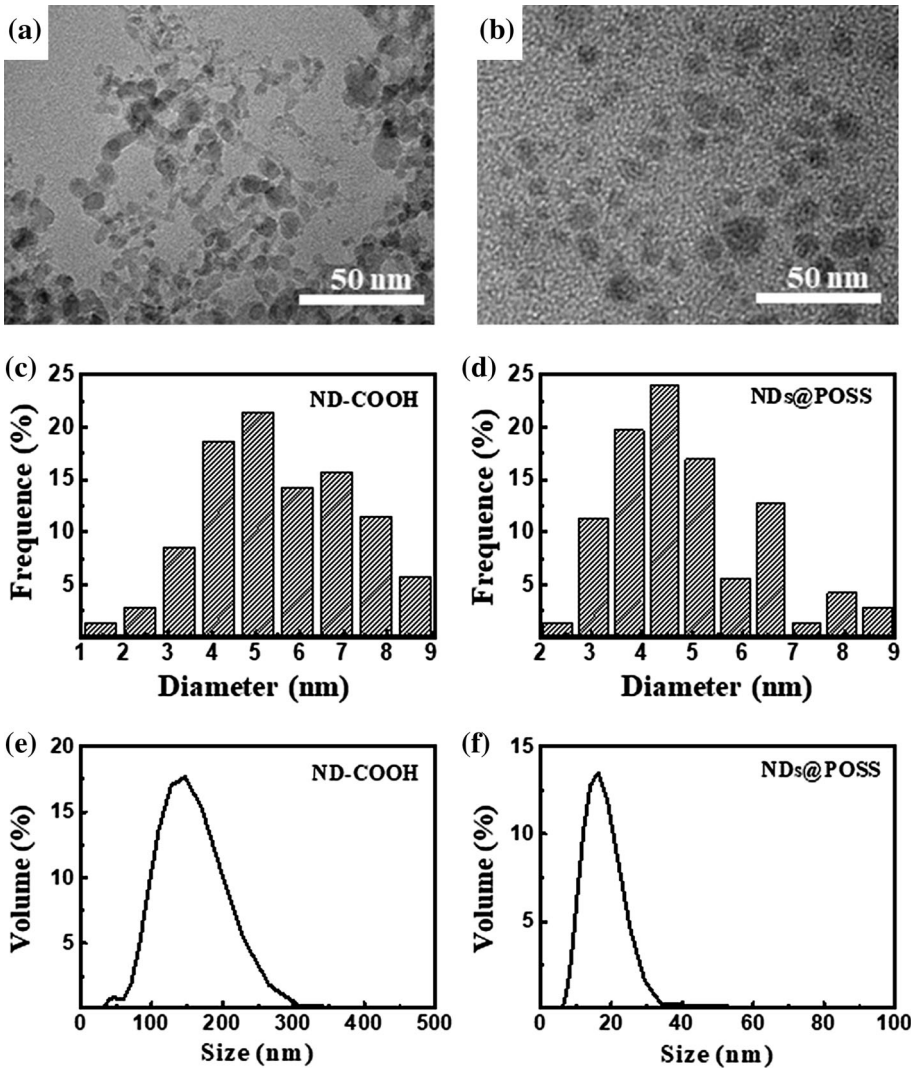

Figure 1 Typical TEM images of **a** ND-COOH and **b** NDs@POSS. Histograms of the particle size distributions for **c** ND-COOH and **d** NDs@POSS obtained from the TEM images. DLS results for the particle size distributions of **e** ND-COOH and **f** NDs@POSS dispersed in toluene.

NDs@POSS, the diameter was less than 10 nm. However, the ND-COOH sample mainly composed of particle aggregates, rather than isolated monodisperse nanoparticles. The NDs@POSS sample exhibited highly dispersive morphology. The size distributions of both ND-COOH and NDs@POSS in toluene were measured by DLS and the results are shown in Fig. 1e, f. The average size of ND-COOH was measured to be 168 nm, while the average size of NDs@POSS in toluene was 13 nm. These results demonstrated that the surface functional groups of POSS on NDs played significant roles in prevent the NDs from aggregation in organic solvents, resulting in much smaller size of NDs@POSS than NDs during DLS measurements.

The samples of ND-COOH and NDs@POSS were further characterized by XRD and FTIR. As shown in Fig. 2a, the ND-COOH exhibited similar diffraction patterns as the ND. Both of them showed two peaks at 43.9° and 75.3°, which were correspond to the diamond core [30]. In addition, a broad peak was observed at around 23°, which was attributed to the sp^2-carbon of amorphous form [31]. The powder of POSS showed amounts of characteristic peaks, indicating the well-defined crystal structure. However, in the XRD profile of the NDs@POSS, a broad peak from 15° to 30° occurred, unlike their pristine POSS counterparts, showing a largely disordered structure with a low crystallinity. These results showed indirect evidence that the POSS molecules were covalently bonded to ND. The FTIR spectra of ND, ND-COOH, POSS, and NDs@POSS are shown in Fig. 2b. There were some changes of ND-COOH as compared to initial NDs. As shown in Fig. 2b, the peaks at

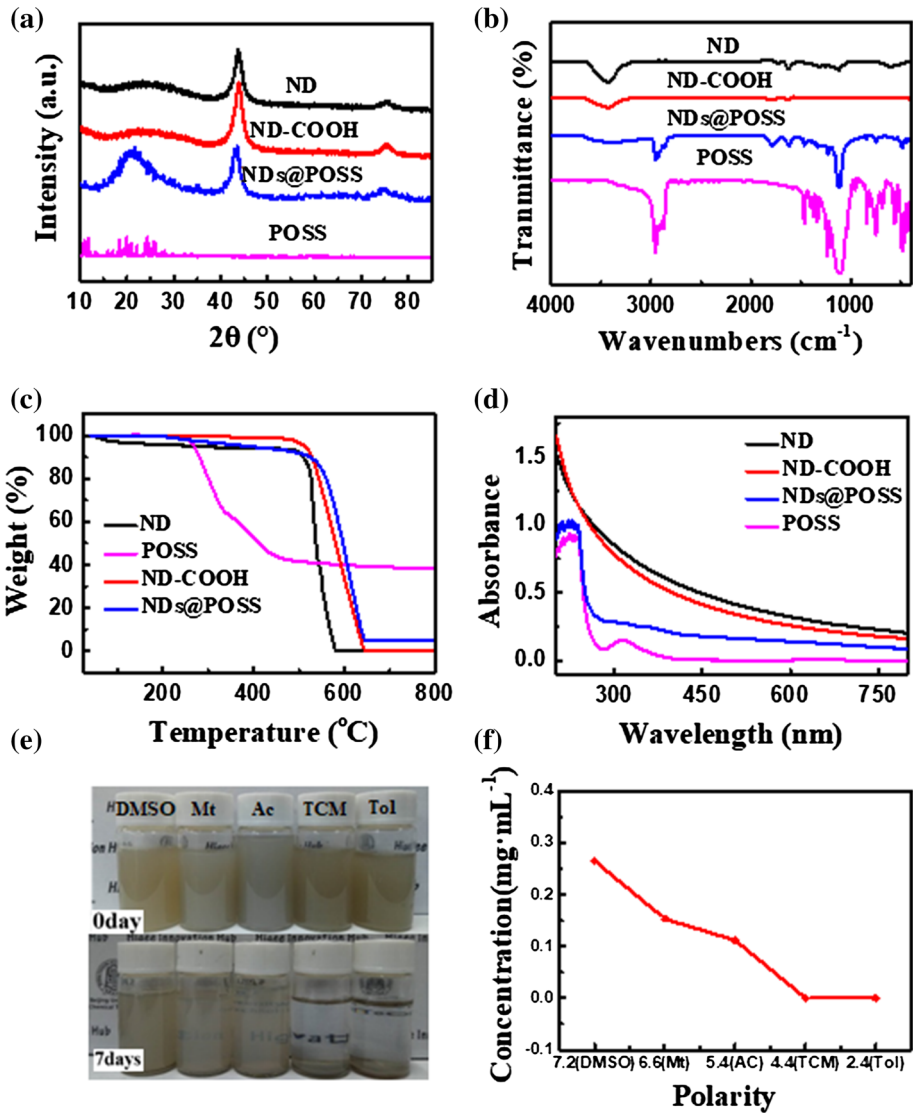

Figure 2 **a** XRD, **b** FTIR, **d** UV–Vis spectra and **c** TGA curves of NDs (black line), POSS (pink line), ND-COOH (red line) and NDs@POSS (blue line). **e** Digital photographs of 1 mg/mL NDs@POSS dispersed in various solvents (up: fresh dispersion; down: stored for 7 days). **f** Relationship between the polarities of the solvents and the contents of NDs@POSS in the suspensions after stored for 7 days. The solvents are dimethyl sulfoxide (DMSO), methanol (Mt), acetone (Ac), trichloromethane (TCM) and toluene (Tol).

3423 cm^{-1} and 1627 cm^{-1} were attributed to the presence of hydroxyl group corresponded to the stretching vibration and to the deformation vibration, respectively. The peak at 1733 cm^{-1} was assigned to the stretching vibration of carbonyl (C=O). In addition to typical FTIR peak, the spectrum revealed another band from oxygen-containing functional groups at 1110 cm^{-1}, which was caused by the stretching vibration C–O–C bond. After oxidation, the C–O–C group in ND disappeared and the C=O band shifted from 1750 to 1798 cm^{-1}, indicating a conversion of ketones, aldehydes, esters and ether groups into the carboxylic acids. The FTIR spectra NDs@POSS showed the presence of a strong peak at 1110 cm^{-1}, due to the Si–O–Si stretching. The relatively weak bands over 2750–3000 cm^{-1} associated with the isobutyl groups in POSS and the peaks at 3423 cm^{-1} and 1627 cm^{-1} attributed to the N–H units, indicated that POSS molecules were chemically grafted onto ND-COOH. The UV–Vis absorption spectra of ND, ND-COOH, POSS, and NDs@POSS are shown in Fig. 2c. Compared to NDs, the ND-COOH exhibited stronger absorption in the ultraviolet due to the increase in the carbonyl structure. The characteristic UV–Vis absorption peaks of POSS are about at 225 nm and 315 nm were observed from NDs@POSS. As the TGA results shown in Fig. 2c, all kinds of carbon including amorphous and diamond phases are quickly oxidized when the temperatures increased up to 450 °C in air. A complete weight loss was observed for both ND and ND-COOH at 650 °C. The residual weight of NDs@POSS at 650 °C (5%) is

higher than the NDs, which was attributed to the highly dense Si–O structure formed by the partial cross-linking of POSS. The NDs/POSS weight ratio in the NDs@POSS nanocomposites was determined to be about 1:9. Figure 2e shows the disperse stability of NDs@POSS in various solvents (from left to right: DMSO, Mt, Ac, TCM and Tol). The polarities of the solvents were: DMSO > Mt > Ac > TCM > Tol (Fig. S1b). The absorbance spectra of the NDs@POSS dispersions in various solvents were measured to investigate the flocculation-settling dynamics. The NDs@POSS could be dispersed well in those solvents to form suspensions under ultrasonic treatment (Fig. 2e). However, after 7 day, significant suspension sediments were observed for the NDs@POSS dispersed in TCM and Tol. The contents of NDs@POSS in various dispersions were monitored by measuring the absorbance of the suspensions. It was found that the larger the polarity of the solvent is, the better the NDs@POSS dispersed (Fig. 2f).

Due to the high refractive index of ND (n = 2.42) [9, 10], one of promising applications of NDs fillers is to make high refractive index polymers. Figure 3a, b shows the transmittance spectra of flexible hybrid films with different concentrations of NDs@POSS embedded in PVB and PC, respectively. Both PVB and PC films showed high transparency in the visible region with transmittance of over 90%. As the increasing of NDs@POSS contents in the hybrid films, the transmittance of the films decreased. The transmittance results of light with wavelength of 550 nm were determined to be 70% for PVB-based hybrid films and 82% for PC-based hybrid films, when the NDs@POSS doping concentration was up to 20 wt% (Fig. S2). The refractive indexes of various films were measured and the results are presented in Fig. 3c, d, in which the refractive index of the hybrid film showed a significant linear correlation with the content of NDs@POSS in the range of 0–20 wt%. The fitting formulas were obtained as $y = 0.2179x + 1.4884$ for NDs@POSS/PVB hybrid films and $y = 0.19044x + 1.57699$ for NDs@POSS/PC hybrid films, respectively. Compared with ZrO_2, one of the commonly used inorganic nanoparticles for preparation of hybrid films with tunable refractive index [32], the ND exhibited higher refractive index. Meanwhile, the ND particles made of earth-abundant carbon, are much greener than PbS which have high refractive index. Therefore, the use of ND-based hybrid films is very promising for further applications. In addition, enhanced thermal stabilities of the hybrid films were observed. The decompose temperatures (T_d) at 10 wt% loss were 172 °C and 320 °C for PVB film and NDs@POSS/PVB hybrid film (Fig. 3e). The decompose temperatures at 10 wt% loss were 400 °C and 440 °C for PC film and NDs@POSS/PC hybrid film, respectively.

Another feature of NDs@POSS nanocomposites was the superhydrophobicity, which was beneficial for the formation of liquid marbles [33–39]. As shown in Fig. S4, NDs@POSS powders showed superhydrophobicity with an air/water contact angle (CA) as high as 154°. A liquid marbles could be simply prepared by rolling water droplets on the powders of NDs@POSS. The self-adsorption and self-assembly process driven by the capillary forces at the water/air interface encapsulated the water droplet and rendered the droplet non-wetting to the substrate [21, 33]. Subsequently, the encapsulating layers of particles were adsorbed on the surface of the liquid marble to form the multilayer. The most notable feature of liquid marbles is “nonstick”. Particles on the surface of liquid droplets can effectively prevent the contact between the internal liquid and the external surface. When the smaller volume drops were rolled, the hydrophobic particles were spontaneously adsorbed at the gas/liquid interface, and the droplet surface could be reduced to form a liquid marble [33]. Figure 4b shows a typical digital photograph of a liquid marble with a diameter of 2 mm prepared from 4 μL water. Figure 4c shows that the liquid marble remained intact after being transferred onto a water bath in a petri dish. The excellent stability of the liquid marble further enabled it to be readily handled with a pair of tweezers owing to elasticity without breaking (Fig. 4d). Compared with the pure droplets, the evaporation rate of the droplets coated by the particles (that was, in the liquid marble) will be reduced. As shown in Fig. 4e, the upper and lower surfaces of the droplets (4 μL) were folded together after the liquid marble was prepared for 45 min.

To investigate the performance of NDs@POSS-based liquid marbles as miniature reactors, two reaction systems were studied. One was the reduction in encapsulated aqueous methylene blue in the presence of sodium borohydride ($NaBH_4$) (Fig. 5). The other one was the reduction in encapsulated aqueous silver ammonia solution in the presence of glucose for the synthesis of Ag nanoparticles. In the initial stage, the presence of the active carboxyl group

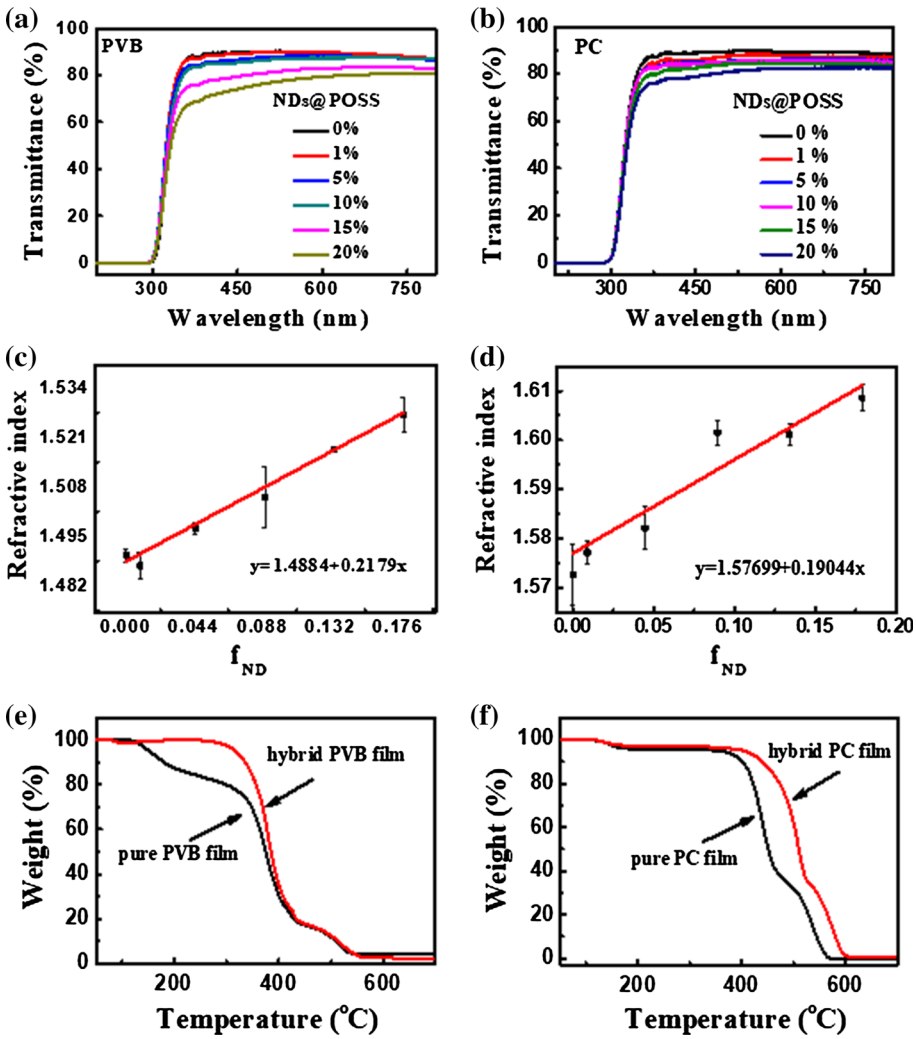

Figure 3 Transmittance spectra of **a** NDs@POSS/PVB films and **b** NDs@POSS/PC films with various contents of NDs@POSS. Dependence curves of the refractive index and the content of NDs@POSS in the hybrid film for **c** NDs@POSS/PVB films and **d** NDs@POSS/PC films. The mass fractions of NDs@POSS were 0, 1, 5, 10, 15, 20%. **e** TGA curves of pure PVB film and NDs@POSS/PVB (10 wt%) hybrid film. **f** TGA curves of pure PC film and NDs@POSS/PC (10 wt%) hybrid film.

on the surface of the NDs makes it deprotonation and produces negative electricity in the basic solution (Fig. S6). Driven by the electrostatic interaction between the negatively charged carboxyl groups and positively charged ions (silver ammonia positive ions and phenothiazine positive ions), the positive ions will be adsorbed on the inner surface of the liquid marbles. When the particles come into contact with the reducing agent in solution, the positive ion reacts by the reduction in electrons. Therefore, the reaction of solutions consists of two processes in a liquid projectile, the adsorption process and reaction process. It should be noticed that the diameter of the liquid marble has an effect on the reaction rate. Typically, the larger the size of the liquid marble was, the lower the active sites inside the surface with reduction in internal surface area were. Considering that temperature, pressure and initial reactant concentration were kept constant throughout the reactions, the increase in the volume of the reaction fluid also contributed to a longer degradation time [36]. In our experiments, for the convenience of sampling, a liquid marble with dimeter of 5 mm was used for the reaction. Figure 5a shows the UV–Vis absorbance spectra of aqueous solution of methylene blue inside liquid marbles without the addition of $NaBH_4$. The results demonstrated that the methylene blue molecules were adsorbed by liquid marbles and reached the adsorption saturation in 5 min. Figure 5b shows the UV–Vis absorbance spectra of 20 μL aqueous solution of methylene blue inside liquid marbles without the addition of $NaBH_4$, in which significant degradation of methylene blue were observed. The mixture solution of methylene blue and $NaBH_4$ in a beaker was also monitored by UV–Vis absorbance spectra measurements, in which the

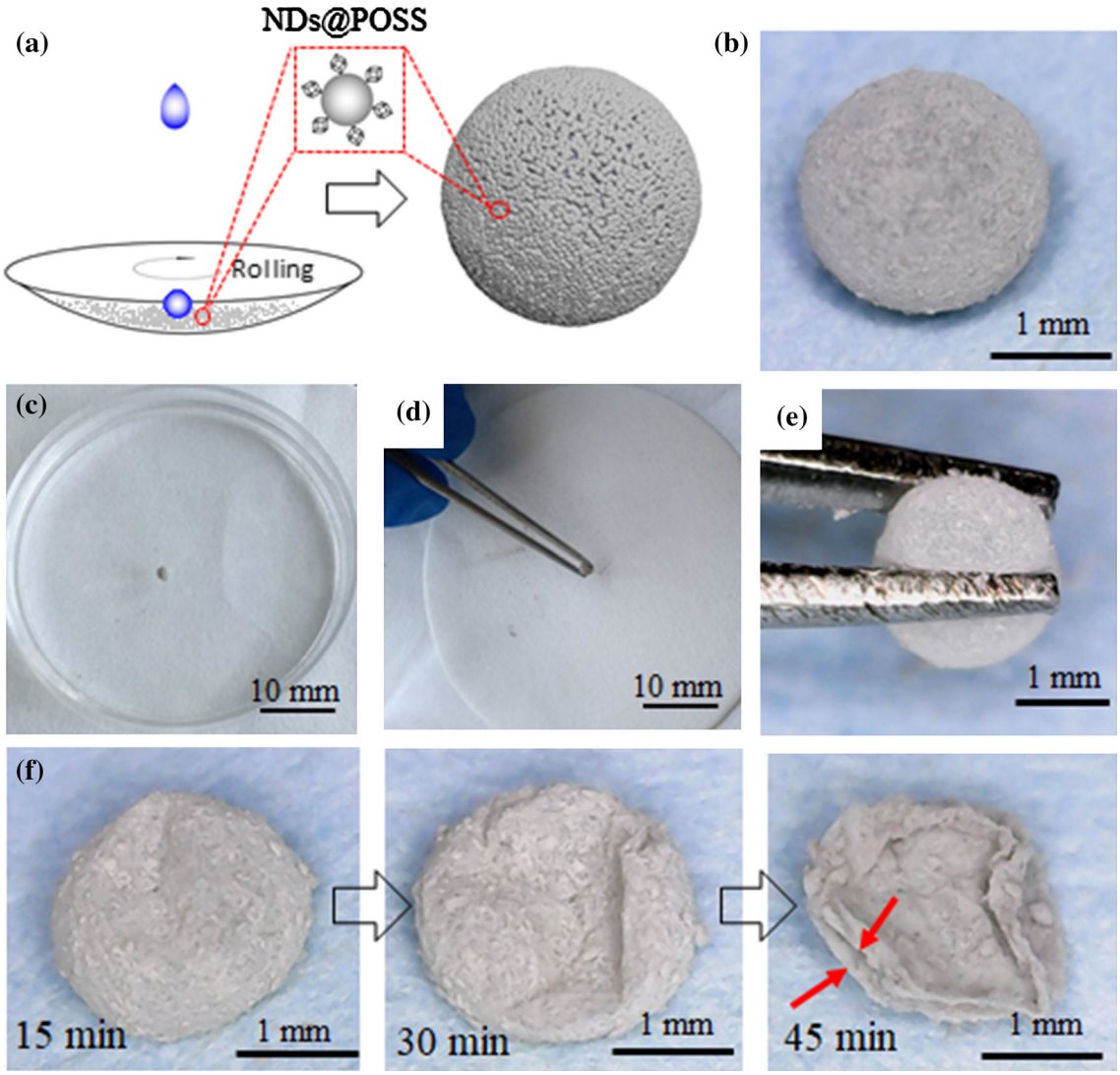

Figure 4 **a** Formation of a liquid marble by rolling a water droplet on NDs@POSS powder. Digital photographs of **b** a liquid marble made from water and NDs@POSS powder (marble size: 2 mm), **c** the liquid marble placed on a water surface, **d** and **e** the liquid marble being picked up with a pair of tweezers. **f** Digital photographs show plan view of the liquid marble during evaporation.

reaction rate was found to be much lower than those in the liquid marbles (Fig. 5c). Figure 5d shows the changes of absorbance intensity of methylene blue in various reactors (liquid marbles and beaker) with and without the addition of $NaBH_4$ at various time points, which indirectly expressed the relationship between the degradation of methylene blue under different conditions. In the initial 5 min, adsorption of methylene blue is the main process. After that, methylene blue degradation was dominant and consumption was 53%. Therefore, the extinction-duration plot depicted an exponential decrease for the methylene blue reacted in the liquid marble. This phenomenon can be due to the electron transfer. In the electron transfer step, when there is a large redox potential difference between acceptor and donor, there may be a case of electron limitation. The NDs@POSS particles distributed on the inner surface of liquid marbles play an electron transfer role as active sites, lowering the original reaction potential [36].

As for the fabrication of Ag nanoparticles using liquid marbles as miniature reactors, similar process intensification effect was demonstrated. With the increase in reaction time, the deposition of silver nanoparticles leads to the gradual deepening of the

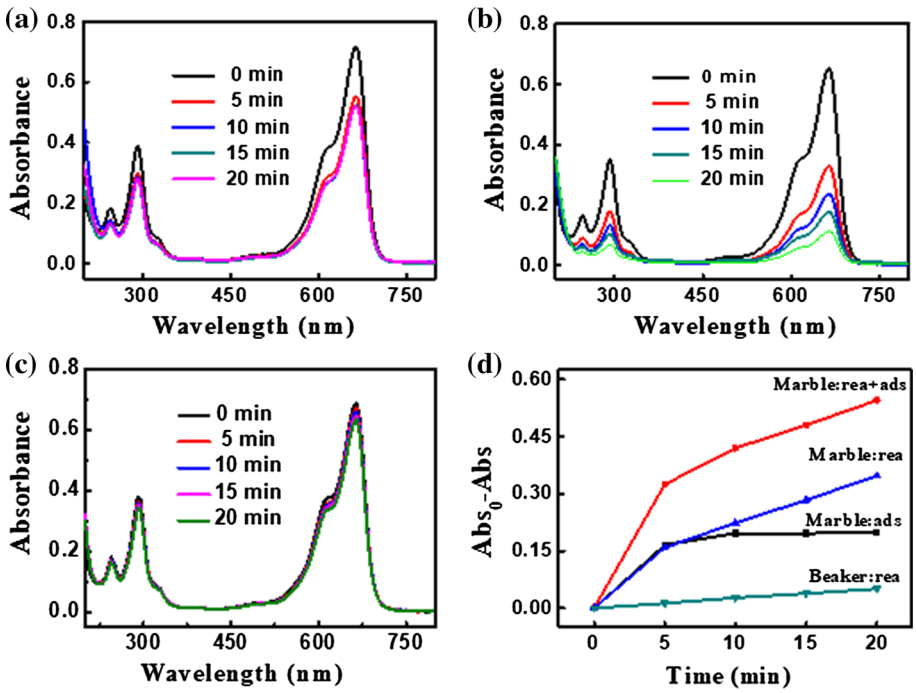

Figure 5 UV–Vis absorbance spectra of aqueous solutions of methylene blue in liquid marbles **a** without the addition of $NaBH_4$ and **b** with the addition of $NaBH_4$ for various time (0, 5, 10, 15 and 20 min). **c** UV–Vis spectra of aqueous methylene blue solution with $NaBH_4$ in a beaker for various time. **d** Changes of the absorbance intensity of methylene blue in various reactors (liquid marbles and beaker) with and without the addition of $NaBH_4$ at various time points. (MB represents for methylene blue).

color of the shell of the liquid marbles. No change in the color of aqueous solution in the liquid marbles was observed in the initial 5 min (Fig. S7), which was attributed to the electrostatic adsorption of silver ammonia positive ions on the inner surface of the liquid marble. And then, the color was deepened on account of the silver mirror reaction preferentially taking place on the encapsulating NDs@POSS nanoparticles. Subsequently, the newly formed Ag^0 could serve as a nucleating site for further formation of Ag nuclei by reducing more Ag^+ around it, leading to the formation of silver mirrors after the growth of silver nuclei. With the formation of the silver mirrors on the inner surface of the liquid marbles, the Ag nanoparticles fall off in the internal solution. After the reaction, the solution was dripped to the Cu grid and tested by TEM. Figure 6b shows the UV–Vis spectra of NDs@POSS and the silver nanoparticles in ethanol solution, and the characteristic absorption peak of silver nanoparticles appears in 430 nm. The silver nanoparticles prepared in liquid marbles showed much smaller sizes than those prepared in a beaker with reactant ratio (Fig. 6c and Fig. S7).

Conclusion

We reported the surface functionalization of NDs with POSS via the covalent bond and performed a series of test characterization. The NDs@POSS nanocomposites were used for multifunctional applications. NDs@POSS nanocomposites-embedded hybrid films were fabricated by solution blending methods, showing tunable refractive indexes in the range of 1.49–1.61. Liquid marbles formed by coating the water droplet with NDs@POSS were prepared as used as miniature reactors for degradation of methylene and fabrication of Ag nanoparticles. The process intensification effects of the NDs@POSS-based miniature reactors were demonstrated. This work represents a new strategy for the design and development of nanodiamonds for multifunctional applications.

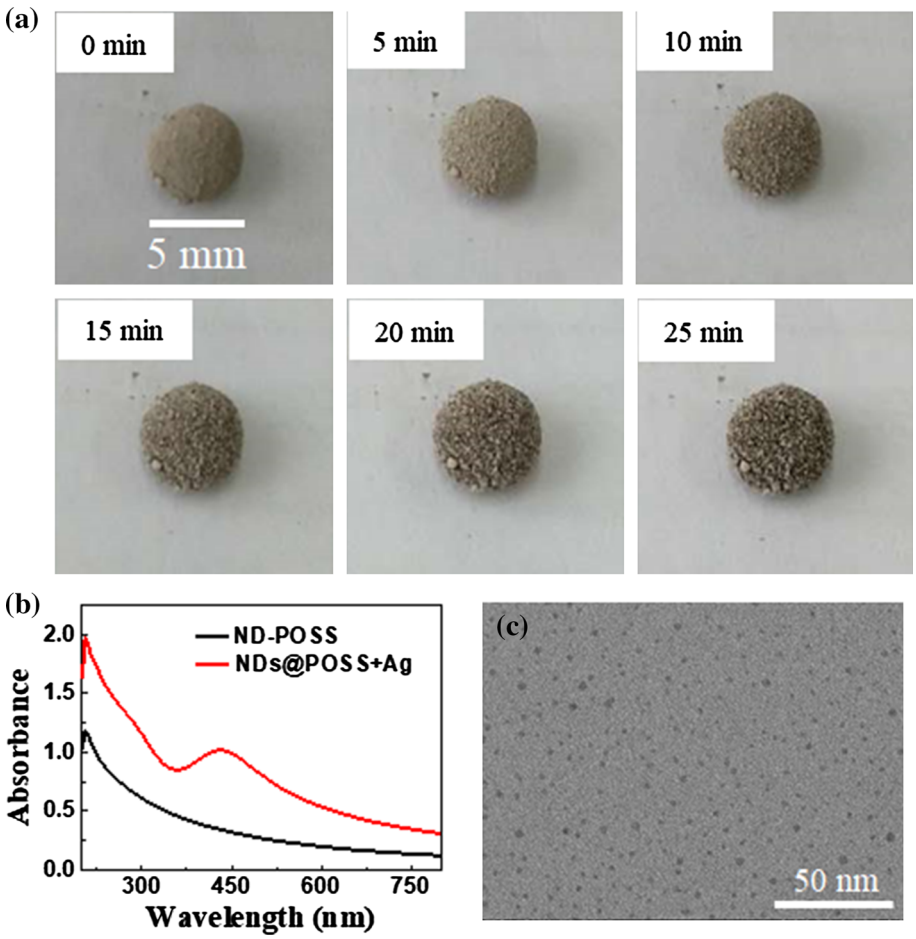

Figure 6 **a** Photographs of a liquid marble with encapsulated ammoniacal silver solution and glucose for the preparation of Ag nanoparticles at various time points from 5 to 25 min. **b** Characteristic absorption curve of silver nanoparticles/NDs@POSS and NDs@POSS. **c** TEM image of Ag nanoparticles prepared in the liquid marble.

Acknowledgements

This work was supported by National Key R & D Program of China (2017YFB0404405/2017YFB0404400).

Compliance with ethical standards

Conflict of interest The authors declare that they have no conflict of interest.

Electronic supplementary material: The online version of this article (https://doi.org/10.1007/s10853-018-2765-7) contains supplementary material, which is available to authorized users.

References

[1] Bartelmess J, Quinn SJ, Giordani S (2015) Carbon nanomaterials: multi-functional agents for biomedical fluorescence and Raman imaging. Chem Soc Rev 44:4672–4698

[2] Wang D, Zhu L, McCleese C, Bruda C, Chen J-F, Dai L (2016) Fluorescent carbon dots from milk by microwave cooking. RSC Adv 6:41516–41521

[3] Wang D, Wang Z, Zhan Q, Pu Y, Wang J-X, Foster NR, Dai L (2017) Facile and scalable preparation of fluorescent carbon dots for multifunctional applications. Engineering 3:402–408

[4] Shen J, Shang S, Chen X, Wang D, Cai Y (2017) Highly fluorescent N, S-co-doped carbon dots and their potential applications as antioxidants and sensitive probes for Cr (VI) detection. Sens Actuators B Chem 248:92–100

[5] Wang Z, Pu Y, Wang D, Shi J, Wang J-X, Chen J-F (2018) 3D-foam-structured nitrogen-doped graphene-Ni catalyst for highly efficient nitrobenzene reduction. AIChE J 64:1330–1338

[6] Aris A, Shojaei A, Bagheri R (2015) Cure kinetics of nanodiamond filled epoxy resin: influence of nanodiamond surface functionality. Ind Eng Chem Res 54:8954–8962

[7] Cao W, Peng X, Chen X, Wang X, Jin F, Li Q, Chen H, Jiang C, Ye Z, Xing X (2017) Facile synthesis of cationic polymer functionalized nanodiamond with high dispersity and

antibacterial activity. J Mater Sci 52:1856–1867. https://doi.org/10.1007/s10853-016-0475-6

[8] Tasaki T, Guo YF, Meng Q, Mamun MAA, Kasahara Y, Akasaka S, Fujimori A (2017) Dependency of nanodiamond particle size and outermost-surface composition on organo-modification: evaluation by formation of organized molecular films and nanohybridization with organic polymers. ACS Appl Mater Interfaces 9:14379–14390

[9] Wang Z, Lu Z, Mahoney C, Yan J, Ferebee R, Luo D, Matyjaszewski K, Bockstaller MR (2017) Transparent and high refractive index thermoplastic polymer glasses using evaporative ligand exchange of hybrid particle fillers. ACS Appl Mater Interfaces 9:7515–7522

[10] Ogata T, Yagi R, Nakamura N, Kuwahara Y, Kurihara S (2012) Modulation of polymer refractive indices with diamond nanoparticles for metal-free multilayer film mirrors. ACS Appl Mater Interfaces 4:3769–3772

[11] Turcheniuk K, Mochalin VN (2017) Biomedical applications of nanodiamond. Nanotechnology 28:252001

[12] Paci JT, Man HB, Saha B, Ho D, Schatz GC (2013) Understanding the surfaces of nanodiamonds. J Phys Chem C 117:17256–172671

[13] Krueger A, Ozawa M, Jarre G, Liang Y, Stegk J, Lu L (2007) Deagglomeration and functionalisation of detonation diamond. Phys Status Solidi 204:2881–2887

[14] Krueger A, Lang D (2012) Functionality is key: recent progress in the surface modification of nanodiamond. Adv Funct Mater 22:890–906

[15] Mochalin VN, Gogotsi Y (2009) Wet chemistry route to hydrophobic blue fluorescent nanodiamond. J Am Chem Soc 131:4594–4595

[16] Maitra U, Jain A, George SJ, Rao CN (2011) Tunable fluorescence in chromophore-functionalized nanodiamond induced by energy transfer. Nanoscale 3:3192–3197

[17] Wang D, Tong Y, Li Y, Tian Z, Cao R, Yang B (2013) PEGylated nanodiamond for chemotherapeutic drug delivery. Diam Relat Mater 36:26–34

[18] Wang D, Li Y, Tian Z, Cao R, Yang B (2014) Transferrin-conjugated nanodiamond as an intracellular transporter of chemotherapeutic drug and targeting therapy for cancer cells. Ther Deliv 5:511–524

[19] Mochalin VN, Neitzel I, Etzold BJ, Peterson A, Palmese G, Gogotsi Y (2011) Covalent incorporation of aminated nanodiamond into an epoxy polymer network. ACS Nano 5:7494–7502

[20] Xue Y, Liu Y, Lu F, Qu J, Chen H, Dai L (2012) Functionalization of graphene oxide with polyhedral oligomeric silsesquioxane (POSS) for multifunctional applications. J Phys Chem Lett 3:1607–1612

[21] Wang D, Liu J, Chen JF, Dai L (2016) Surface functionalization of carbon dots with polyhedral oligomeric silsesquioxane (POSS) for multifunctional applications. Adv Mater Interfaces 3:1500439

[22] Gomathi A, Gopalakrishnan K, Rao CNR (2010) Covalent functionalization of metal oxide and carbon nanostructures with polyoctasilsesquioxane (POSS) and their incorporation in polymer composites. Mater Res Bull 45:1894–1898

[23] Kunthom R, Jaroentomeechai T, Ervithayasuporn V (2017) Polyhedral oligomeric silsesquioxane (POSS) containing sulfonic acid groups as a metal-free catalyst to prepare polycaprolactone. Polymer 108:173–178

[24] Han J, Zheng Y, Zheng S, Li S, Hu T, Tang A, Gao C (2014) Water soluble octafunctionalized POSS: all-click chemistry synthesis and efficient host–guest encapsulation. Chem Commun 50:8712–8714

[25] Xiang K, Li Y, Xu C, Li S (2016) POSS-based organic–inorganic hybrid nanomaterials: aggregation-enhanced emission, and highly sensitive and selective detection of nitroaromatic explosives in aqueous media. J Mater Chem C 4:5578–5583

[26] Ma Y, He L, Jia M, Zhao L, Zuo Y, Hu P (2017) Cage and linear structured polysiloxane/epoxy hybrids for coatings: surface property and film permeability. J Colloid Interface Sci 500:349–357

[27] Wang D, Zhu L, Chen JF, Dai L (2016) Liquid marbles based on magnetic upconversion nanoparticles as magnetically and optically responsive miniature reactors for photocatalysis and photodynamic therapy. Angew Chem Int Ed 55:10795–10799

[28] Xue Y, Wang H, Zhao Y, Dai L, Feng L, Wang X, Lin T (2010) Magnetic liquid marbles: a "precise" miniature reactor. Adv Mater 22:4814–4818

[29] Molavi H, Shojaei A, Pourghaderi A (2018) Rapid and tunable selective adsorption of dyes using thermally oxidized nanodiamond. J Colloid Interface Sci 524:52–64

[30] Turcheniuk K, Trecazzi C, Deeleepojananan C, Mochalin VN (2016) Salt-assisted ultrasonic deaggregation of nanodiamond. ACS Appl Mater Interfaces 8:25461–25468

[31] Baidakova MV, Kukushkina YA, Sitnikova AA, Yagovkina MA, Kirilenko DA, Sokolov VV, Shestakov MS, Vul AY, Zousman B, Levinson O (2013) Structure of nanodiamonds prepared by laser synthesis. Phys Solid State 55:1747–1753

[32] Xia Y, Zhang C, Wang J-X, Wang D, Zeng X-F, Chen J-F (2018) Synthesis of transparent aqueous ZrO_2 nanodispersion without modification for high-refractive-index nanocomposite film. Langmuir 34:6806–6813

[33] Mchale G, Newton MI (2011) Liquid marbles: principles and applications. Soft Matter 7:5473–5481

[34] Mchale G, Newton MI (2015) Liquid marbles: topical context within soft matter and recent progress. Soft Matter 11:2530–2546

[35] Koh C, Lee HK, Phan-Quang GC, Han X, Lee MR, Yang Z (2017) SERS- and electrochemically-active 3D plasmonic liquid marble for molecular-level spectroelectrochemical investigation of microliter reaction. Angew Chem Int Ed 56:8813–8817

[36] Miao YE, Lee HK, Chew WS, Phang IY, Liu T, Ling XY (2014) Catalytic liquid marbles: Ag nanowire-based miniature reactors for highly efficient degradation of methylene blue. Chem Commun 50:5923–5926

[37] Sheng Y, Sun G, Ngai T (2016) Dopamine polymerization in liquid marbles: a general route to janus particles synthesis. Langmuir 32:3122–3129

[38] Shang Q, Hu L, Hu Y, Liu C, Zhou Y (2018) Fabrication of superhydrophobic fluorinated silica nanoparticles for multifunctional liquid marbles. Appl Phys A 124:25

[39] Sheng Y, Sun G, Wu J, Ma G, Ngai T (2015) Silica-based liquid marbles as microreactors for the silver mirror reaction. Angew Chem Int Ed 54:7012–7017